Experimental and numerical investigation of the effect of vertical loading on the lateral behaviour of monopiles in sand

Li, Q.; Gavin, K. G.; Askarinejad, A.; Prendergast, L. J.

DOI
10.1139/cgj-2020-0769

Publication date
2022

Document Version
Final published version

Published in
Canadian Geotechnical Journal

Citation (APA)
Li, Q., Gavin, K. G., Askarinejad, A., & Prendergast, L. J. (2022). Experimental and numerical investigation of the effect of vertical loading on the lateral behaviour of monopiles in sand. *Canadian Geotechnical Journal*, *59*(5), 652-666. https://doi.org/10.1139/cgj-2020-0769

Canadian Science Publishing

ARTICLE

Experimental and numerical investigation of the effect of vertical loading on the lateral behaviour of monopiles in sand

Q. Li, K.G. Gavin, A. Askarinejad, and L.J. Prendergast

Abstract: The influence of combined loading on the response of monopiles used to support offshore wind turbines (OWTs) is investigated in this paper. In current practice, resistance of monopiles to vertical and lateral loading is considered separately. As OWT size has increased, the slenderness ratio (pile length, L, normalised by diameter, D) has decreased and foundations are tending towards intermediate footings with geometries between those of piles and shallow foundations. Whilst load interaction effects are not significant for slender piles, they are critical for shallow footings. Previous research on pile load interaction has resulted in conflicting findings, potentially arising from variations in boundary conditions and pile slenderness. In this study, monotonic lateral load tests were conducted in a geotechnical centrifuge on vertically loaded monopiles in dense sand. Results indicate that for piles with L/D = 5, increasing vertical loading improved pile initial stiffness and lateral capacity. A similar trend was observed for piles with L/D = 3, when vertical loading was below ≈45% of the pile's ultimate vertical capacity. For higher vertical loads considered, results tended towards the behaviour observed for shallow footings. Numerical analyses conducted show that changes in mean effective stress are potentially responsible for the observed behaviour.

Key words: combined loading, monopiles, sand, centrifuge modelling, lateral soil resistance – displacement (p–y) curves.

Résumé : Cet article étudie l'influence des charges combinées sur la réponse des monopiles utilisés pour soutenir les éoliennes en mer (OWT). Dans la pratique actuelle, la résistance des monopieux aux charges verticales et latérales est considérée séparément. Avec l'augmentation de la taille des OWT, le rapport d'élancement (longueur du pieu, L, normalisée par le diamètre, D) a diminué, et les fondations tendent vers des semelles intermédiaires dont la géométrie se situe entre celle des pieux et celle des fondations superficielles. Alors que les effets d'interaction des charges ne sont pas significatifs pour les pieux minces, ils sont critiques pour les semelles peu profondes. Les recherches antérieures sur l'interaction entre les charges sur les pieux ont donné lieu à des résultats contradictoires, qui peuvent être dus à des variations des conditions limites et de l'élancement des pieux. Dans cette étude, des essais de charge latérale monotone ont été réalisés dans une centrifugeuse géotechnique sur des monopieux chargés verticalement dans du sable dense. Les résultats indiquent que pour les pieux avec L/D = 5, l'augmentation de la charge verticale améliore la rigidité initiale du pieu et sa capacité latérale. Une tendance similaire a été observée pour les pieux avec L/D = 3, lorsque la charge verticale était inférieure à ≈45 % de la capacité verticale ultime du pieu. Pour les charges verticales plus élevées considérées, les résultats tendent vers le comportement observé pour les semelles peu profondes. Les analyses numériques effectuées montrent que les changements de la contrainte effective moyenne sont potentiellement responsables du comportement observé. [Traduit par la Rédaction]

Mots-clés : chargement combiné, monopieux, sable, modélisation par centrifugeuse, courbes de résistance latérale du sol – déplacement (p–y).

1. Introduction

The development of offshore wind turbines (OWTs) has experienced rapid growth in recent years and is considered the most mature technology to facilitate the energy transition (Li et al. 2018). Monopiles remain the most commonly used foundation to support OWTs accounting for 87% of all installations to 2019 (WindEurope 2018; Fan et al. 2021). Monopiles comprise single open-ended steel tubes driven into the seabed. Typical pile sizes used to support early OWTs had diameters, D, in the range 4–6 m and embedded lengths, L, in the range 20–30 m, with L/D between 5 and 6 (Doherty and Gavin 2012). As turbines grow to 10 MW, the pile diameter required to limit pile mudline rotation is increasing to between 8 m and 10 m (Byrne et al. 2019). The combination of relatively low turbine weight and large pile diameter means embedded lengths of monopiles have not increased significantly and L/D ratios have reduced towards values in the range 2–3. Although referred to as monopiles, these are more correctly termed intermediate foundations, which are classified in ISO 1990-1-4 (ISO 2016) as having L/D in the range 1–10.

Several authors have studied combined loading for shallow and skirted foundations. Interaction effects can occur such that

Received 7 January 2021. Accepted 28 July 2021.

Q. Li. Faculty of Civil Engineering and Geosciences, Delft University of Technology, Building 23, Stevinweg 1/P.O. Box 5048, 2628 CN Delft/2600 GA Delft, the Netherlands; Huadong Engineering (Shenzhen) Corporation Limited, Shenzhen, China.
K.G. Gavin and A. Askarinejad. Faculty of Civil Engineering and Geosciences, Delft University of Technology, Building 23, Stevinweg 1/P.O. Box 5048, 2628 CN Delft/2600 GA Delft, the Netherlands.
L.J. Prendergast. Department of Civil Engineering, Faculty of Engineering, University of Nottingham, Nottingham, NG7 2RD, UK.
Corresponding author: L.J. Prendergast (email: luke.prendergast@nottingham.ac.uk).

Table 1. Model and corresponding prototype pile dimensions and properties of test piles.

		Model					Prototype*		
Pile ID	Strain gauge	L_T (mm)	E (GPa)	D (mm)	t (mm)	L/D	E (GPa)	D (m)	L/D
P1	10 pairs	240	70	18	1	5	210	1.8	5
P2	None	240	70	18	1	5	210	1.8	5
P3	None	204	70	18	1	3	210	1.8	3

*Assuming prototype pile is fabricated from steel and g-level = 100g.

Fig. 1. Photograph of model monopiles: (*a*) P1 and (*b*) P3 (unit: millimetre). [Colour online.]

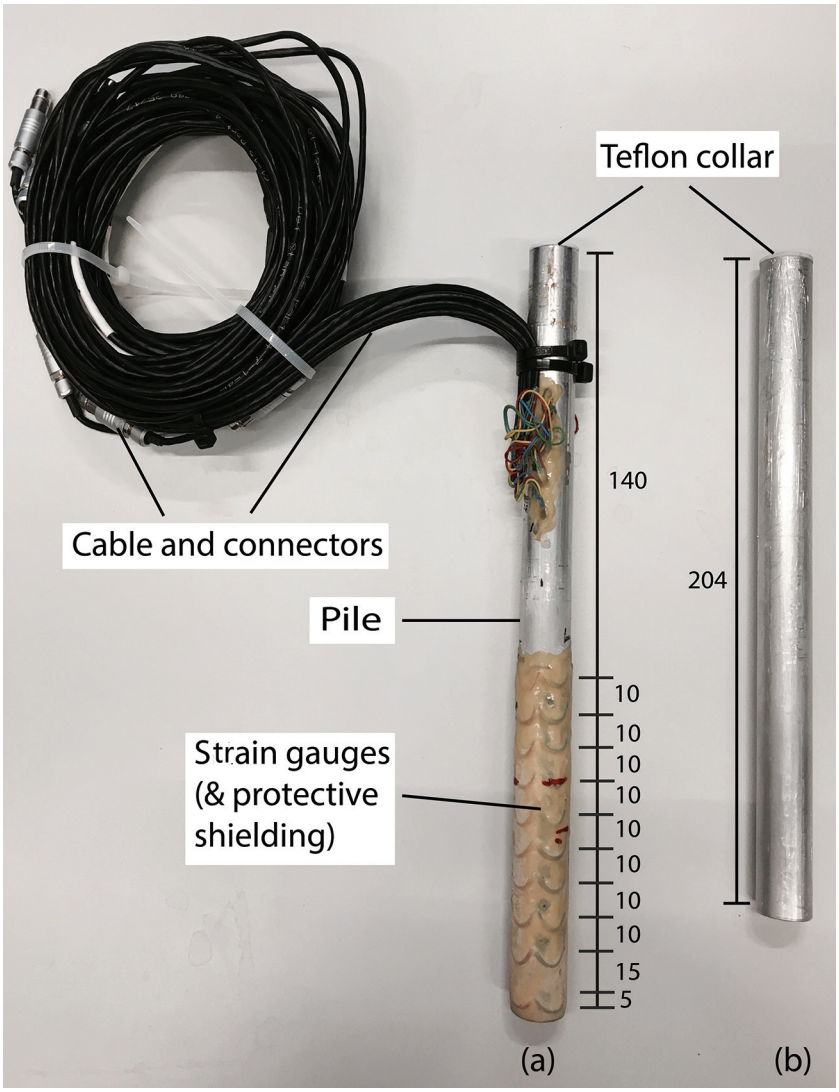

the lateral load, H, and moment, M, capacity of footings depend on the current vertical load level, V (Nova and Montrasio 1991; Butterfield and Gottardi 1994; Bransby and Randolph 1998). Whilst a number of studies have considered load-interaction effects on piles, very few have investigated monopile behaviour. Karasev et al. (1977) conducted full-scale combined load tests on cast-in-place concrete piles (D = 600 mm, L = 3 m, and L/D = 5) in sandy loam. Test results indicate that vertical loads have a beneficial effect on the lateral load response of piles (the lateral displacement of piles was observed to decrease considerably with increasing vertical load). Jain et al. (1987) performed laboratory combined load tests on fully and partially embedded long flexible open-ended piles (D = 32 mm, L = 1000 mm and L/D = 31.25) installed in sand with a relative density (D_r) of 78%. They reported that the application of vertical loads increased lateral displacements of the pile. Lee (2008) performed laboratory pile tests to assess the influence of vertical loading on the lateral response of piles in sand. Installation effects were considered by testing driven and non-displacement piles. Tests were performed in sand where D_r varied between 38% and 91%. The piles had D = 30 mm, L = 1100 mm, and L/D of 37. Similar to the findings of Jain et al. (1987), the authors observed that lateral displacements of the pile head increased with increasing vertical load. Mu et al. (2018) performed combined load tests in a geotechnical centrifuge, where the monopile had D = 6 m, L = 50 m, and L/D = 8.3 (at prototype scale) installed in fine, dry sand with relative density of 79%. Strain gauges

Fig. 2. Sketch of pile.

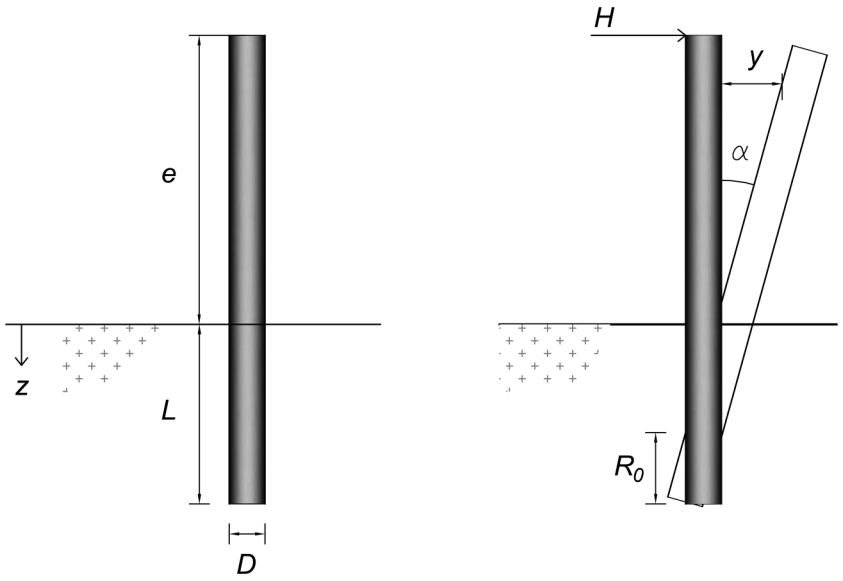

were installed on the pile to study the influence of vertical loading on the bending moment and lateral soil resistance – displacement (p–y) curves. It was found that the presence of vertical loading decreased the lateral displacement of the monopile. Lu and Zhang (2018) reported centrifuge tests where combined loads were applied to a pile with D = 1 m, L = 16.5 m, and L/D = 16.5. They also found that lateral displacements measured at a given applied lateral load decreased as the vertical load increased.

In summary, Karasev et al. (1977), Mu et al. (2018), and Lu and Zhang (2018) suggested that the presence of vertical loading improves pile performance (reduces lateral displacements). In contrast, Jain et al. (1987) and Lee (2008) reported the opposite effect. The nature of the response appears to be a trade-off between the p-delta influence, whereby vertical loads applied to laterally displaced piles induce additional moments exacerbating deflections; and vertical loads increasing the stiffness at the pile-soil interface subsequently reducing lateral deflections. Additional reasons for this discrepancy might be related to variations in the pile top fixity applied in the experiments and the range of L/D considered. There is further uncertainty surrounding how the sequence of load application, soil density and soil type influence the responses. Notwithstanding the contradictory results, there is a dearth of data, which consider pile performance under a range of vertical loads, L/D ratios, and installation methods under controlled loading and soil conditions. Interested readers are referred to Li et al. (2020*b*) for a comprehensive review of the topic.

In this paper, the effect of vertical loading on the lateral response of monopiles used to support OWTs is examined using centrifuge testing. The effect of pile slenderness ratios typically adopted for OWTs on the lateral load capacity and p–y curves for monopiles installed in dense sand is studied. To assess the impact of installation stress on the pile response, a series of tests are compared where piles are both installed in-flight and pre-installed.

2. Experimental methodology

2.1. Facility and model monopile instrumentation

The experiments in this paper were undertaken using the beam centrifuge at Delft University of Technology (Allersma 1994; Li et al. 2020*c*; Zhang and Askarinejad 2019*b*). A brief summary of the testing is provided herein. Three aluminium tubular model piles with outer diameter, D = 18 mm and wall thickness, t = 1 mm were fabricated, termed herein as P1, P2, and P3. To create the scaled models, similitude between the flexural stiffness (EI) of the prototype and model piles is conserved. The properties of these piles at both model and prototype scales are provided in Table 1. P1 was instrumented with ten strain gauges while P2 and P3 were not instrumented. The gauges and cables on P1 are protected by a 0.5 mm thick layer of epoxy coating, which increases the pile wall thickness and roughness. This may result in a larger pile lateral resistance in the experiments conducted. A photograph of the instrumented pile (P1) and one un-instrumented pile (P3) is shown in Fig. 1.

Table 2. Geotechnical properties of Geba sand (De Jager et al. 2017; Maghsoudloo et al. 2018).

e_{min}	e_{max}	Gs	D_{50} (mm)	C_C	C_U	φ_{cr} (°)
0.64	1.07	2.67	0.11	1.24	1.55	35

The piles simulate a 1.8 m diameter steel pipe pile with t = 30 mm at prototype scale (tested at 100g), and were installed by jacking to L/D ratios of 3 or 5. It should be noted that the prototype dimensions are smaller than those typically observed for offshore piles, this is a result of the limitations in the permissible pile geometry to avoid boundary effects (elaborated below) and the maximum acceleration field that can be implemented in the centrifuge. However, the slenderness ratio is within the expected range. The terminology used to describe the pile response is summarized in Fig. 2; L refers to pile embedded length, e is loading eccentricity, R_0 is distance from the pile pivot point to the pile toe, H is applied lateral load, y is pile lateral displacement at any height along the pile, and α is pile rotation angle. The loading eccentricity, e, was maintained constant in all tests at 8D.

2.2. Soil preparation and characterisation

Piles were installed in dense dry Geba sand with D_r = 80% formed using an air pluviation technique. The geotechnical parameters of Geba sand are provided in Table 2 (Maghsoudloo et al. 2018). The critical state friction angle (φ_{cr}) is 35°, which is obtained from drained triaxial tests performed on sand specimens with D_r = 80% up to an axial strain of at least 20% (~17.7% shear strain). The silica sand is quite sub-angular. The ratio of outer pile diameter to average grain size of the sand (D/D_{50}) is approximately 164, which is sufficient to avoid particle size effects (Nunez et al. 1988; Dyson and Randolph 2001; Garnier

Fig. 3. Schematic showing in-flight pile installation procedures: (*a*) initial installation of the pile to 2*D* embedment depth at 1g; (*b*) pile in-flight installation (5*D* embedment depth shown as an example); (*c*) raising of actuator to accommodate subsequent lateral load test.

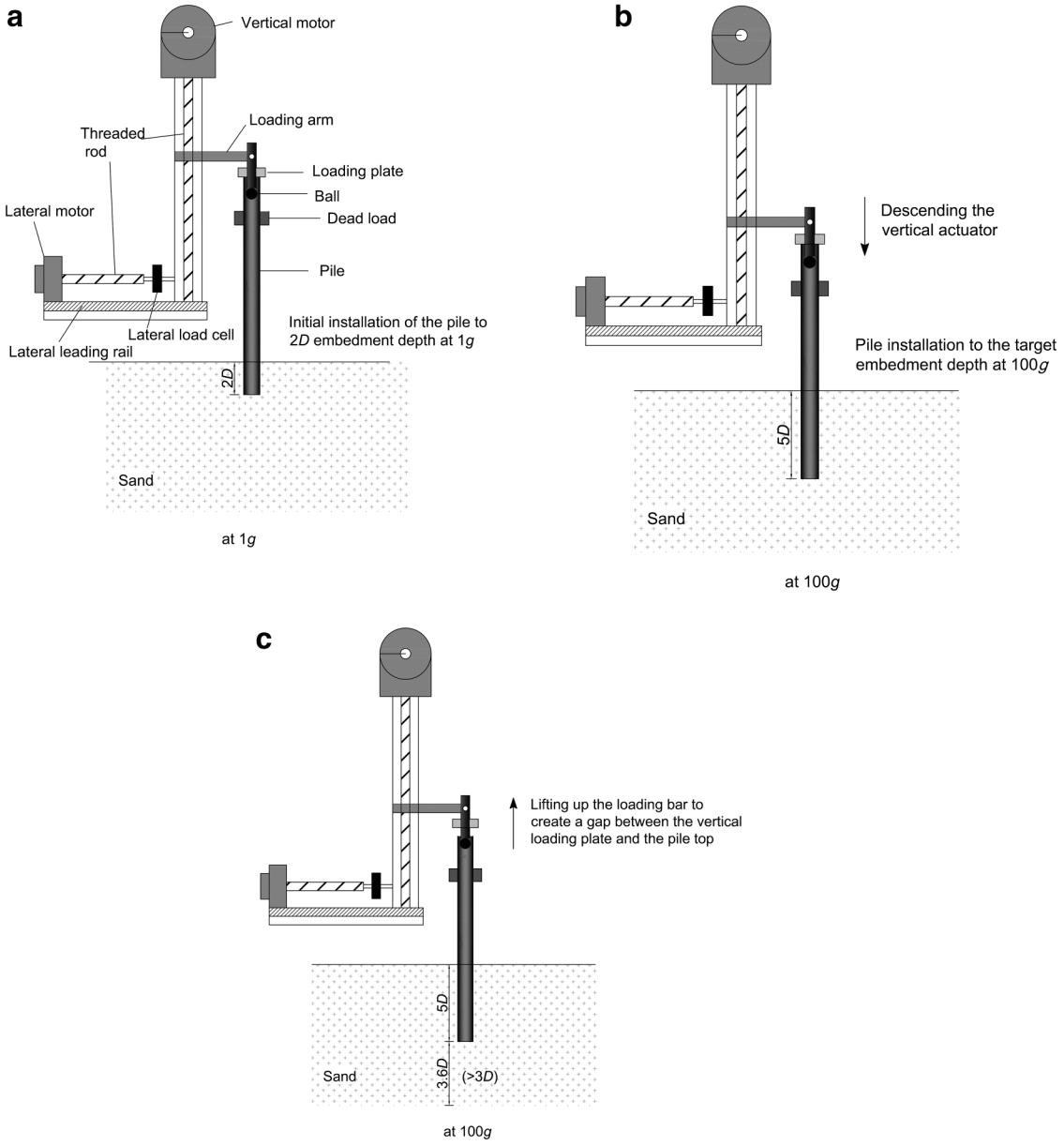

et al. 2007; Klinkvort and Hededal 2010; Zhang and Askarinejad 2019*a*). The ratio of wall thickness to mean particle size t/D_{50} is 9.1, which is very close to the suggested limiting value of 10 (De Nicola 1996; De Nicola and Randolph 1997) to avoid particle-size effects from influencing the interaction between the pile annulus and the soil. The plan dimensions of the sand sample are 410 mm by 150 mm, with a sample depth of 155 mm. The ratio of the smallest size of the box to the pile diameter is 8.3, which is larger than the limiting value of 4 as suggested by Prakasha et al. (2005). For the largest pile embedment ratio ($L/D = 5$), the distance from the pile tip to the bottom of the strong box is 3.6*D*, which is larger than the minimum value of 3*D* required to avoid boundary effects (Prakasha et al. 2005). It should be noted that for centrifuge testing there is a trade-off between how large the distances to the boundaries can be while still using an appropriately large pile model to obtain sensible results. It is acknowledged that the distances to the boundaries, though larger than suggested in Prakasha et al. (2005), are still quite minimal in the present work. A brief numerical study was undertaken to ascertain if the boundaries of the present model adversely influenced the findings, and the results suggested that their influence is minimal — more information is provided in Section 4 of the paper.

2.3. Pile installation and test procedure

Piles were installed using a displacement-controlled actuator at a rate of 0.05 mm/s. The instrumented pile P1 was jacked to its final penetration depth 5*D* at 1g (to avoid potential damage to the strain gauges and connecting cable by the high stresses when installing at 100g). The remaining uninstrumented piles were jacked to an initial depth of 2*D* at 1g to maintain vertical stability at elevated g-levels, see Fig. 3*a*. Following this initial jacking, the centrifuge was spun-up to 100g and the piles were jacked to their final embedment depth 5*D* (P2) and 3*D* (P3), see Fig. 3*b*.

Installing piles by jacking in place at 1g or in-flight at 100g deviates from what would typically occur offshore, whereby piles are typically impact-driven to penetration, which results

Fig. 4. Ball connection for reducing pile-head constraint (dimensions in millimetres).

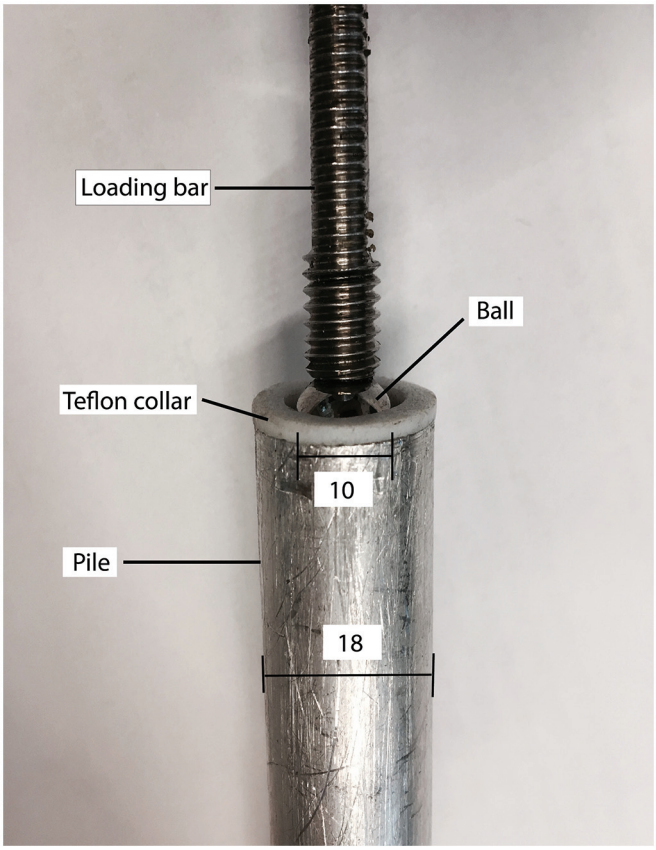

in potential differences in mobilised residual base stresses that might be developed in the real case. It was not possible to install the piles by driving at 100*g* as this would require stopping the centrifuge to adjust the loading rig for the subsequent lateral load application, which would add uncertainty surrounding the influence of the sample stress history on the results obtained (Li et al. 2020*c*). It is noteworthy that the mobilisation of residual stresses may lead to additional base moments on the piles when subjected to lateral loading (Murphy et al. 2018), which are not encountered in the present case. Dyson and Randolph (2001) and Fan et al. (2021) have shown that pile installation method (in-flight driven and jacking) exhibits a reasonable impact on the pile lateral resistance (around 10%–20%). The results in this paper consider piles with the same installation approach so the global differences between driven and jacked are less important, but the results should still be considered in this regard.

A friction-reducing ball connection (Li et al. 2020*a*) was used to transfer lateral loads produced by the actuator to the pile head, see Fig. 4. The ball was placed vertically into the open end of the pile head, where it rested in contact with the internal wall of the pile. Between the pile inner surface and the ball, a Teflon collar was used to minimize interface friction.

In the combined loading tests, the vertical load (V) was fixed on the pile using dead weights prior to pile installation. During the combined loading tests, the lateral load (H) for the pile installed at 1g was monitored at the pile head by parallel beam load cells (HTC-SENSOR TAL220, HT Sensor Technology Co., Ltd. 2021) with a measuring range of ±100 N and sensitivity 0.05%, see Fig. 5.

To perform lateral tests following in-flight installation without stopping the centrifuge, a load cell with measurement capacity of 200 N (SIMBATOUCH SBT650 2021) was placed between the lateral motor and vertical loading tower, see Fig. 3*a*. The parallel beam load cell cannot be used in this test program, due to the potential high bending moment caused by pile vertical installation. The vertical and lateral displacements of the pile at the loading position (pile head) can be monitored by vertical and lateral motor encoders, which have an accuracy of approximately 3×10^{-5} mm. Any compliance within the system is assumed minimal as the movements of the pile are expected to be significantly larger than these.

The experimental programme comprises 14 centrifuge tests, summarised in Table 3. Tests are described using pile number, acceleration level during installation, and test type/nature. For example, P1-1g-L1 refers to the first lateral load test performed on pile P1, installed at 1g. Each test was conducted twice to ensure repeatability. The initial stiffness during each test, k_{ini}, is also documented in Table 3.

3. Experimental results

3.1. Vertical load–displacement response

The vertical load capacity, V_u, of each pile is firstly determined by means of load testing, corresponding to the first two cases in Table 3. For piles installed in flight (P2 and P3), V_u was defined as the vertical load (jacking force) required to achieve the target penetration. Figure 6 shows the results of the vertical load vs displacement response for piles P1–P3, and it can be seen that the results from repeat tests are consistent (the repeat test for P1 is also consistent but is omitted from the plot for clarity). The vertical capacity for P3, with L/D = 3, is 12 MN; and P2, with L/D = 5, is 20 MN. It should be noted that for piles P2 and P3, the vertical load vs displacement response exhibits an increased slope for penetrations exceeding 6D. This possibly occurs as a result of boundary effects whereby the pile tip approaches the location of the bottom of the box. The effect of installation method is evident from the initial stiffness of P1. For consistency, V_u of P1 is assumed to be equal to P2 in subsequent analyses.

3.2. Lateral load–displacement response under vertical loading

In this section, lateral load–displacement behaviour of each pile for each of the cases detailed in Table 3 is reported.

The effect of installation stress is considered in Fig. 7, where lateral load-displacement response curves for the piles with L/D = 5 are shown. The pile installed in-flight (P2-100*g*-L1) exhibits both larger initial stiffness (k_{ini}) and lateral resistance than that of the pile pre-installed at 1g (P1-1g-L1). This suggests retention of high mean effective stresses caused by the installation process affects the lateral load-displacement response even at very large lateral displacements. When the pile was installed in-flight, the amount of surface heave is reduced which leads to greater densification of the sand over the upper few diameters (Dyson and Randolph 2001). The inner filling ratio (plug length of the sand divided by the pile embedment length) was ≈55%. In the pre-installed case, fully coring behaviour was observed (no plugging). The same trend is evident in Fig. 7 for combined load tests where the vertical load was fixed at 0.225V_u. It is suggested that results might be valid for smaller diameter piles with intermediate embedment, as well as large-diameter monopiles.

The ultimate lateral load capacity H_u is defined as the resistance developed when the pile head displacement at the mudline level reaches 0.1D (Lee 2008). Although both piles in Fig. 7 are seen to develop lateral resistance that increase with displacement, H_u is defined as 0.64 and 0.93 MN for P1 and P2, respectively.

The influence of vertical loading on the lateral load-displacement response for the piles installed to L/D = 5 are compared in Fig. 8. It is apparent that an increase in vertical load resulted in an increase in both initial stiffness and lateral capacity of each pile. This trend is broadly similar for piles pre-installed at 1g and jacked at 100g within the mudline lateral pile displacement range 0 to 0.1D.

The likely mechanism controlling the increase in initial stiffness and the lateral capacity in the presence of vertical loading is

Fig. 5. Picture of arrangement of testing components on the instrumented pile (pile P1). [Colour online.]

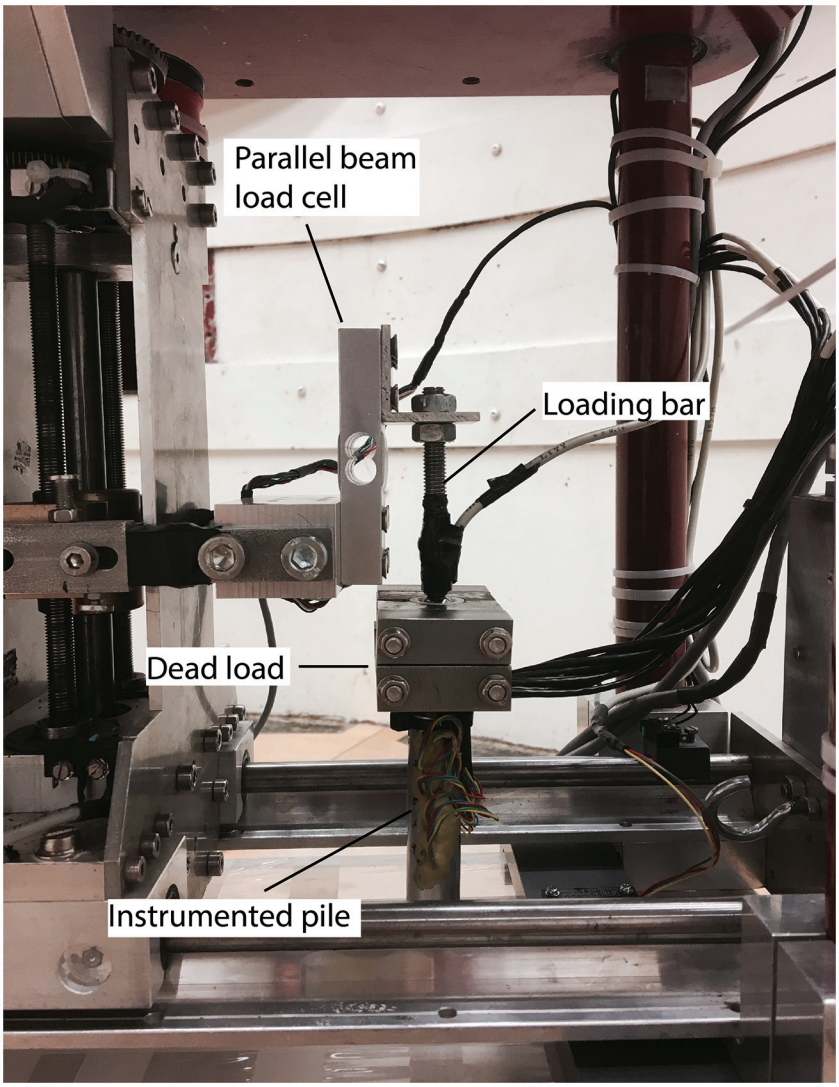

the increased mean effective stress level in the sand caused by the pre-application of vertical loads. This causes an increase in sand stiffness and strength thereby increasing lateral resistance (Karthigeyan et al. 2007; Lu and Zhang 2018), which is investigated numerically in Section 4. The experimental results presented in Fig. 8 are consistent with the centrifuge study of Mu et al. (2018) and Lu and Zhang (2018).

The influence of vertical loading on the lateral load–displacement response for piles installed to $L/D = 3$ is shown in Fig. 9 (see Table 3). The data show that the initial stiffness increased with the application of vertical loading. Pile lateral resistance also increased up to a lateral mudline displacement of approximately $0.05D$. For the tests with applied vertical loads of 0, $0.27V_u$, and $0.55V_u$, lateral resistance continued to increase with increasing lateral displacement. However, the rate of increase for the pile with a vertical load of $0.27V_u$ is higher than for the pile with $0.55V_u$, such that at mudline displacement $y/D = 0.1$, the lateral capacity measured in both tests was approximately equal. In the test where the applied vertical load is $0.82V_u$, the resistance reduces for mudline displacements larger than $0.05D$, and the H_u value at mudline displacement $y/D = 0.1$ is only slightly higher than the pile with no vertical load. From the data it is clear that L/D and V/V_u have an influence on the load-interaction response of monopiles.

The influence of vertical loading on the pile lateral capacity (H_u) can be expressed by the following equation (Karthigeyan et al. 2007; Mu et al. 2018):

$$\vartheta = H_{u,V}/H_{u,0} \quad (1)$$

where ϑ is normalized pile lateral capacity; $H_{u,V}$ is pile lateral capacity when applied vertical load is nonzero; and $H_{u,0}$ is pile lateral capacity under lateral loading only ($V = 0$). The data in Fig. 9 make it clear that ϑ is very sensitive to the mudline displacement y/D value at which the pile lateral capacity is defined.

A summary of the ϑ values from all tests is shown in Fig. 10, which reveals

1. For the range of parameters considered, ϑ is always greater than unity, meaning the application of vertical loading reduces corresponding lateral displacements.
2. For piles with $L/D = 3$, lateral capacity increases initially as vertical load increases. The normalized pile lateral capacity reaches a peak value when the vertical load is between $0.4V_u$ and $0.5V_u$. For higher loads the beneficial effect of vertical loading reduces. A parabolic failure locus similar in shape to those reported for shallow foundations by Nova and Montrasio (1991) appears to match the pile response well. However, for

Table 3. Summary of pile test programme.

Test number	Pile L/D	Test nature	Vertical load	k_{ini} (MN/m)
P2/P3-100g-V	2*	Obtain vertical capacity (V_u)	0 to V_u	—
P1-1g-V	5†			
P1-1g-L1	5	Assess influence of vertical	0	9.2
P1-1g-L2	5	loading on lateral capacity	$0.15V_u$	10.2
P1-1g-L3	5		$0.225V_u$	11.5
P1-1g-L4	5		$0.3V_u$	12.2
P2-100g-L1	5	Assess influence of vertical	0	11.5
P2-100g-L2	5	loading on lateral capacity	$0.225V_u$	13.1
P2-100g-L3	5		$0.45V_u$	15.3
P2-100g-L4	5		$0.675V_u$	16.7
P2-100g-L5	5		$0.9V_u$	20.4
P3-100g-L6	3		0	1.8
P3-100g-L7	3		$0.27V_u$	3.6
P3-100g-L8	3		$0.55V_u$	4.9
P3-100g-L9	3		$0.82V_u$	7.6

*Pile has 2D initial embedment before the vertical load test begins.
†Pile has 5D initial embedment before the vertical load test begins.

shallow foundations discussed in Nova and Montrasio (1991), the lateral capacity is zero when the applied vertical load is zero (assuming the foundation weight can be ignored and there is no embedment) ($V = 0$, $H = 0$). When applied vertical loads increase, the bearing stress between the foundation and subsoil increases, which increases the lateral capacity through mobilised friction ($0 < V < V_u$, $0 < H$). However, when applied vertical loads surpass a certain threshold, post-failure conditions occur and lateral capacity is reduced to zero ($V = V_u$, $H = 0$). This fundamentally differs from pile behaviour whereby lateral capacity largely depends on pile rigidity, therefore even when applied vertical loads are zero, pile lateral capacity is a non-zero value ($V = 0$, $0 < H$).

3. For piles with L/D of 5, pile lateral capacity increases non-linearly with increasing vertical loads, and the benefit increases as vertical load level increases. At a given V/V_u the beneficial effect is smaller than that seen on the pile with $L/D = 3$ for V/V_u below 0.8.
4. Comparing data for P1 and P2 with $L/D = 5$, the results are very sensitive to the V_u chosen for the normalisation. Whilst V_u was measured directly for P2 and P3 as the jacking force required for installation, see Fig. 6, P1 was jacked at 1g and thus the V_u that should be adopted in the normalisation is not straight-forward to define. A vertical load test performed in-flight from an initial embedment depth of 5D on this pile is shown in Fig. 11. It is clear that a very large displacement of 0.9D was required to mobilise V_u of 20 MN adopted for consistency with P2 (thus the pile embedment length is 5.9D). An alternative definition of V_u that might be more in keeping with the stress state effective at the time of the lateral load test is to define V_u as the point at which pile stiffness decreases significantly in the vertical load test. From Fig. 11 an alternative definition of V_{u_pre} for P1 is 6.5 MN. Replotting the data in Fig. 10 with this lower V_u value shows comparable behaviour with P2.

3.3. Influence of vertical loading on *p*–*y* curves for monopiles

In this section, the impact of vertical loading on the lateral soil reaction-displacement (p–y) curves mobilised along the depth of P1 is discussed.

p–y curves can be derived from bending moment profiles, where p is derived by double differentiation of the moment profile, and y at discrete locations is obtained by double integration of the moment profile, see Li et al. (2021) for procedure. The rotation point is assumed at 0.7L along the pile (Fan et al. 2021; Chortis et al. 2020).

Given double differentiation propagates measurement errors it is common to apply curve fitting techniques to minimise these errors, see Xue et al. (2016). Polynomial curve-fitting method (Yang and Liang 2006) is adopted for curve-fitting the moment data. A 5th order polynomial is used to generate soil reaction (by differentiation) and a 7th order polynomial is used to obtain soil displacements (by integration).

Using this approach, p–y curves derived from the bending moment profile for test P1-1g-L1 ($V = 0$) are shown in Fig. 12. The normalised lateral displacement profiles seen in Fig. 12*a* show that the pile lateral displacement (y) is almost linearly distributed demonstrating rigid pile behaviour, with "toe-kick" (Achmus 2010; Chortis et al. 2020) evident below the rotation point. The corresponding normalised soil reaction profiles along the pile are shown in Fig. 12*b* with large resistance mobilised at the pile toe. The data can be combined in the form of p–y curves in Fig. 12*c*, which show that the lateral resistance and stiffness increase with depth as expected. It should be noted that the p–y curve nearest the point of rotation is difficult to extract due to the low lateral

Fig. 6. Determination of the vertical load capacity of the tested piles. [Colour online.]

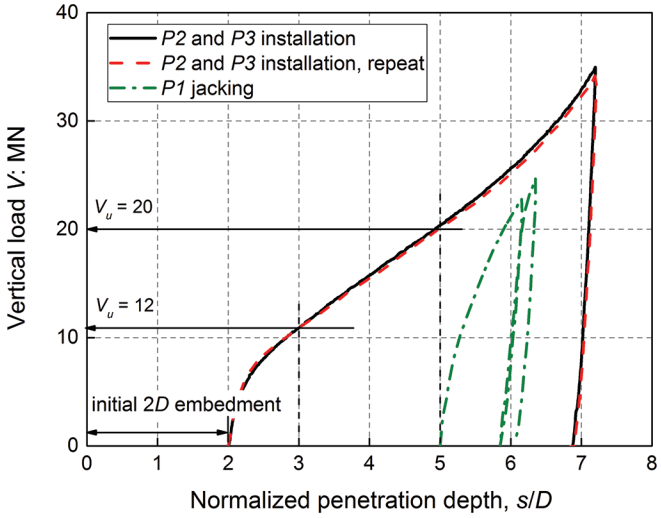

Fig. 7. Influence of pile installation stress level on the lateral load–displacement relationship ($L/D = 5$). [Colour online.]

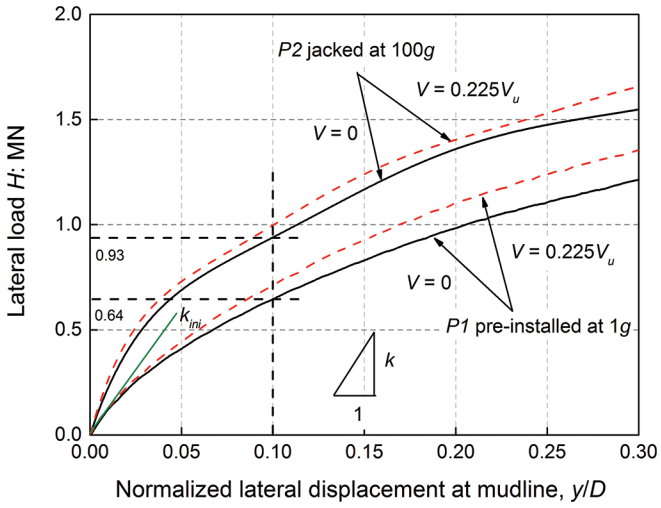

Fig. 8. Influence of vertical loading on the lateral load-displacement relationship: piles pre-installed at 1g and jacked at 100g (L/D = 5). [Colour online.]

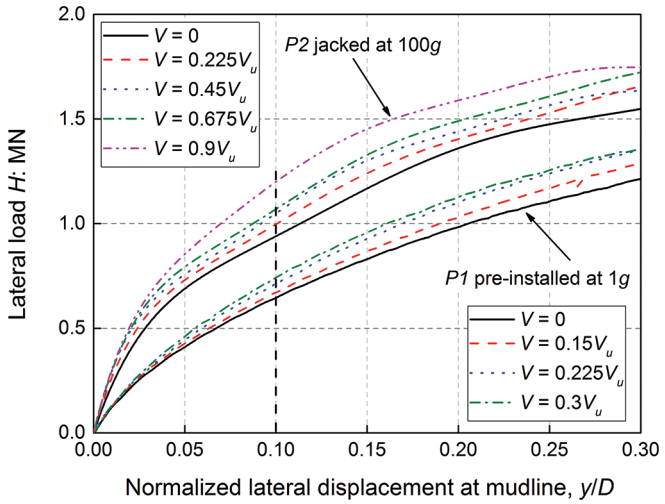

Fig. 9. Influence of vertical loading on the lateral load–displacement relationship for pile jacked at 100g (L/D = 3). [Colour online.]

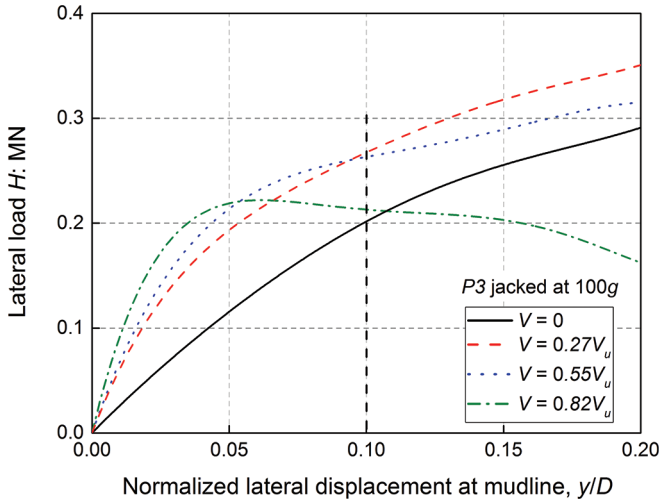

Fig. 10. Influence of vertical loading on the lateral capacity of the model piles. [Colour online.]

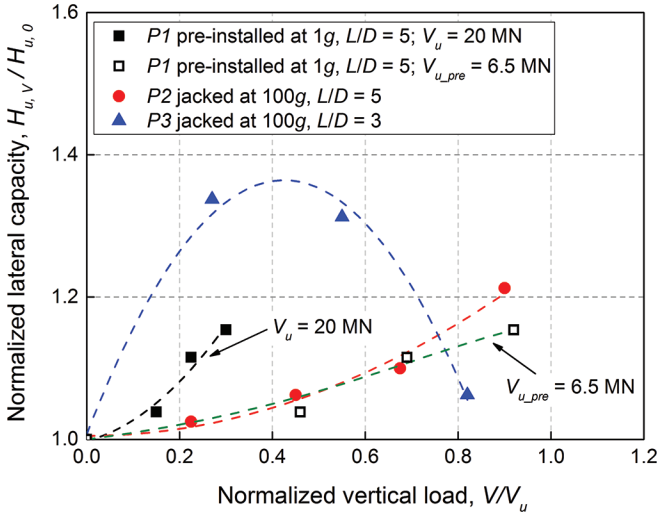

Fig. 11. Vertical load–displacement relationship on the pre-installed pile (L/D = 5). [Colour online.]

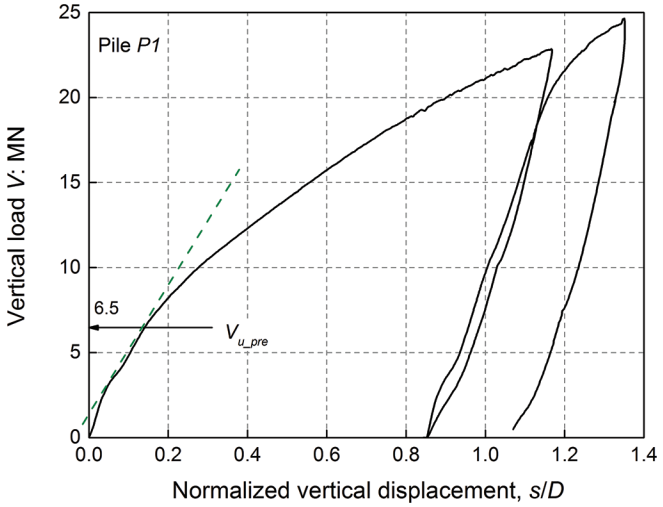

displacements experienced by the pile at this location. There is therefore likely some error present with the curve closest this location, in this particular case, the curve at depth 7 m. Similar observations have been reported in other literature (Chortis et al. 2020).

Figures 13*a*–13*d* show the influence of vertical load level on the normalized derived p–y curves at increasing depths, from z = 2 to 5 m, respectively. It is evident that the stiffness and normalised soil reaction (p/D) generally increase as the vertical load level increases from 0 to 0.3 V_u.

Mu et al. (2018) suggest the influence of applied vertical loading on the soil resistance can be quantified using the following equation:

$$\chi = \frac{p_V - p_0}{p_0} \quad (2)$$

where χ is the improvement in lateral soil resistance at some reference displacement level due to the application of vertical loading, p_0 is the lateral soil resistance under zero vertical loading, and p_V is the lateral soil resistance when the applied vertical load is nonzero. Considering Fig. 13*a* (z = 2 m) and taking y/D = 0.01 as the reference displacement level, the normalised soil reaction p_V/D increases by 13%, 16%, and 20% over the p_0/D value as the vertical load increases to 0.15 V_u, 0.225 V_u and 0.3 V_u respectively. Similar data from all soil depths are summarised in Fig. 14, which shows an approximately linear increase of χ as the vertical load level increases. This figure demonstrates the improvement in soil resistance measured under increasing vertical load.

It is of interest to compare the derived p–y curves in the present study with those prescribed in offshore design codes, such as the American Petroleum Institute (API 2011). The API curves were originally derived from load tests on relatively slender piles. Recognising the limitations for rigid monopiles, several authors have derived p-y curves for piles of varying geometries. Choo and Kim (2016) proposed experimental p-y curves based on centrifuge tests of 6 m diameter monopiles (at prototype scale) installed in dense sand. Qi et al. (2016) conducted a series of centrifuge tests at a scale of 1:250 to investigate the influence of scour erosion on the lateral behaviour of piles. The model pile used has an equivalent prototype diameter of 2.75 m and an embedded depth of 31.25 m.

Fig. 12. Derivation of *p*–*y* curves for test P1-1g-L1 (V = 0): (*a*) displacement profiles, (*b*) soil reaction profiles, and (*c*) *p*–*y* curves.

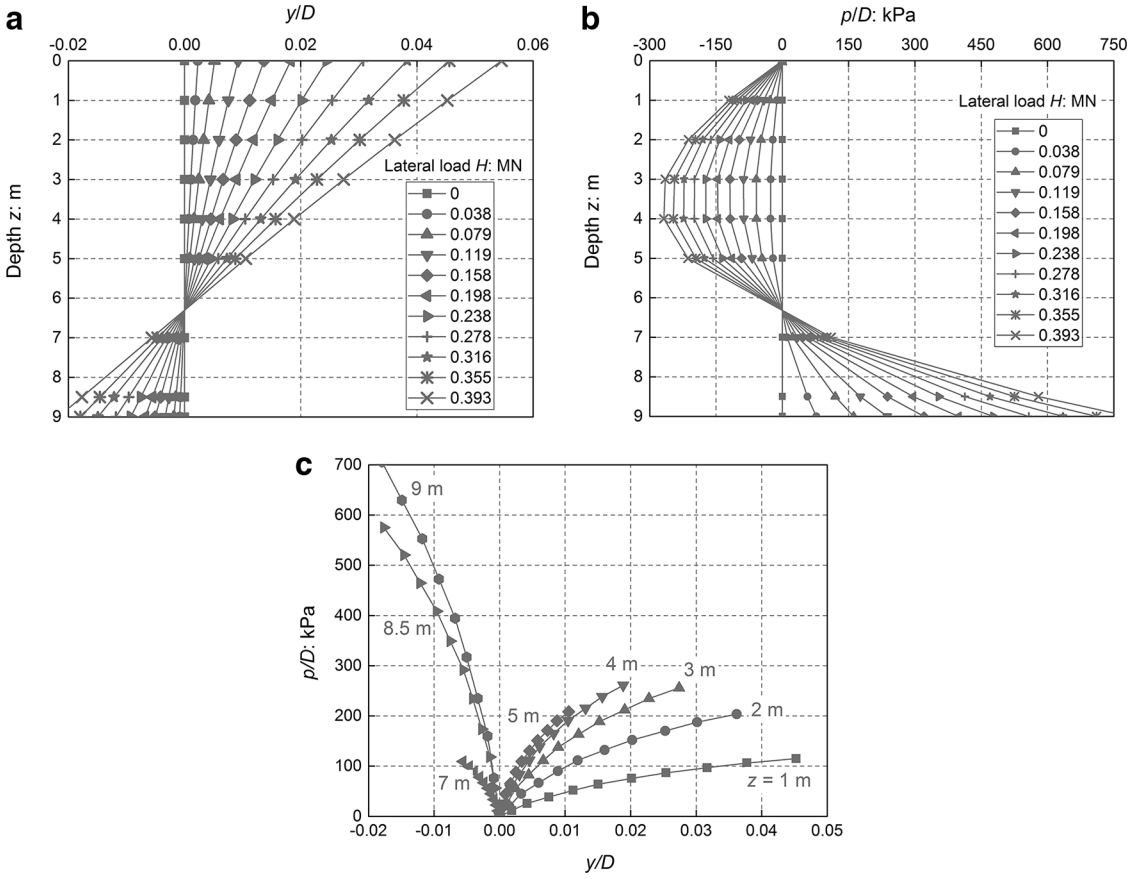

The *p*-*y* curves derived experimentally in this paper were compared with those from API (2011), Choo and Kim (2016), and Qi et al. (2016). To facilitate comparison across scales, p was normalized by $\gamma' D^2$ and y was normalized by D. These curves at a normalized soil depth of $z = 2D$ are shown in Fig. 15. The *p*–*y* curves from this paper correspond well to the *p*–*y* curve from the pile with L/D = 7.1 from Choo and Kim (2016), which was installed in a single layer of dense sand with D_r = 82%–86%. The *p*–*y* curve derived by Qi et al. (2016) on the other hand exhibits very soft behaviour, though the pile tested has a larger L/D (= 11.4).

For the API *p*–*y* curves, "failure" is reached at a relatively small lateral displacement (e.g., 0.008D). The initial stiffness and strength of the API *p*–*y* relationship are much greater than those determined from the centrifuge experiments.

The experimental data in Fig. 15 suggests that the *p*–*y* response is very sensitive to L/D. This is in keeping with the results of major experimental and numerical test programmes such as the recently completed PISA project (Byrne et al. 2019; McAdam et al. 2019). Considering the significant difference between the *p*–*y* curves determined from the centrifuge experiments and the API recommendations, further large-diameter rigid pile tests should be carried out to formulate the database for establishing design criteria.

4. Numerical analysis

In this section, the phenomena leading to the observed results in the previous sections are investigated numerically. PLAXIS 3D (Brinkgreve et al. 2015), is used to perform the finite-element (FE) simulations.

4.1. Model

The 3D FE mesh used for the analysis of pile-soil interaction with associated geometrical properties is shown in Fig. 16. A model domain width of 20D, length of 40D, and distance below pile tip of 20D was generated, to ensure no boundary effects influenced the results. A comparative model developed with the same boundary distances as the prototype dimensions in the centrifuge tests exhibited only minor effects from boundaries, but this study could not be used to quantify the influence of boundaries due to differences in the chosen stress points between both models. Due to the ease of modelling, the larger model was used in subsequent analyses. Only half the pile section is modelled and a refined mesh is adopted near the pile with a coarser mesh adopted elsewhere. Lateral boundaries are considered smooth and the bottom surface is considered rough. Dry sand was used in the simulations.

Analyses are performed on a single free-headed steel pipe wished-in-place pile in sand. The pile top comprises a rigid plate to enable the application of vertical loads, and the top metre of sand within the pile is removed to prevent interactions occurring. The pile is assumed to be linear elastic with E = 210 GPa and ν = 0.3. A Hardening Soil model is used to model the sand, where the parameters are derived based on D_r = 80% (Brinkgreve et al. 2010). Table 4 provides the pile and soil parameters. The relative strength of the interface to the strength of the soil (R_{inter}) is set as 0.7. It should be noted that representative sand parameters are used in the model but it is not intended to model the exact conditions from the experimental tests. Therefore, only qualitative results are sought in this section.

4.2. Change in mean effective stress under vertical loading only

To investigate the mechanism underlying the observed increase in lateral capacity under applied vertical loads, the change in mean

Fig. 13. Influence of vertical loading on normalized *p*–*y* curves at various depths (*a*, *b*, *c*, *d*: *z* = 2–5 m, respectively). [Colour online.]

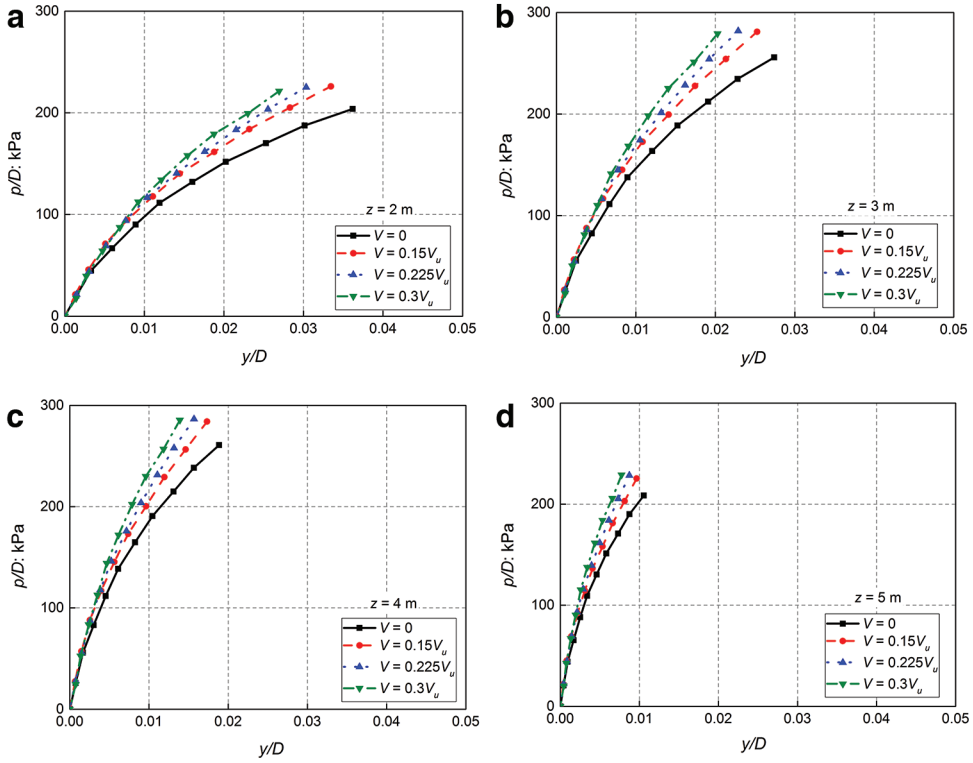

Fig. 14. Improvement in soil resistance under applied vertical load (at *y* = 0.01*D*). [Colour online.]

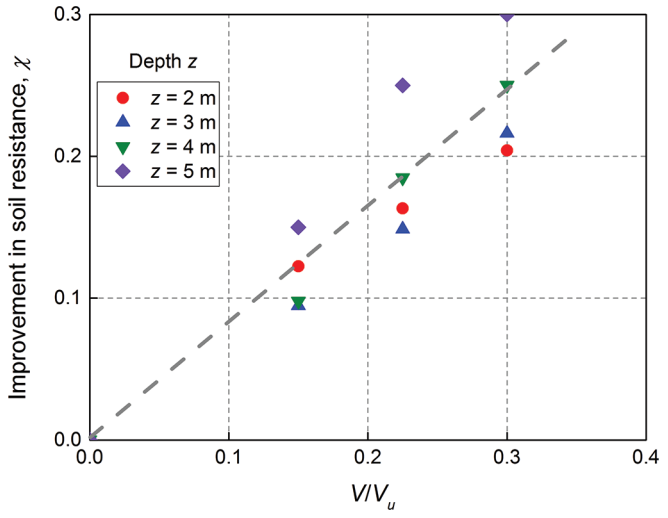

Fig. 15. Comparison of normalized *p*-*y* relationships obtained in this study with those from previous literature at a normalized depth *z* = 2*D*. [Colour online.]

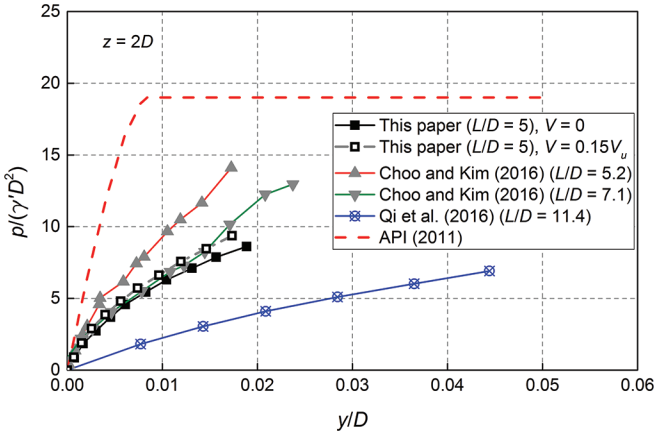

effective stress levels around the pile is calculated herein. Under the action of vertical loading only, the change in mean effective stress level measured near the pile in the *XZ*-plane is shown in Fig. 17 for piles with *L*/*D* of 5 and 3. The change in mean effective stress is obtained by subtracting the mean effective stress profile corresponding to the initial unloaded condition from that corresponding to the applied vertical load of $0.2V_u$, where V_u is obtained by loading the pile in a separate simulation. The mean effective stress level increases substantially in the region surrounding each pile once the vertical loading is applied, suggesting that lateral stiffness and strength will also be increased, offering a potential qualitative explanation of the observed behaviour in the experimental tests.

Under the action of vertical loading only, the change in mean effective stress level in the *XY*-plane is shown in the supplementary material section (see Fig. S1[1]), corresponding to a depth of 1.5*D* (2.7 m) in the ground. Figure S1*a*[1] shows the data for the pile with *L*/*D* = 5, and Fig. S1*b*[1] shows that for the pile with *L*/*D* = 3. This plot demonstrates the increase in mean effective stress generated around both piles due to the application of vertical loading, and moreover shows that at a given distance from each pile, the

[1]Supplementary data are available with the article at https://doi.org/10.1139/cgj-2020-0769.

Fig. 16. Typical mesh adopted in three-dimensional finite element analysis. [Colour online.]

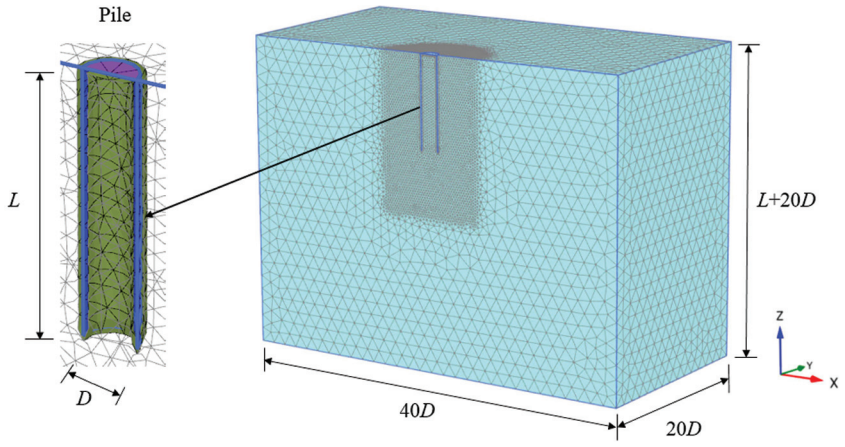

Table 4. Pile geometries and soil properties.

Pile No.	Diameter, D (m)	Embedded length, L (m)	L/D ratio	Wall thickness, t (mm)
1	1.8	5.4	3	30
2	1.8	9	5	30

D_r	γ (kN/m^3)	E_{50}^{ref} (kN/m^2)	E_{oed}^{ref} (kN/m^2)	E_{ur}^{ref} (kN/m^2)	m	ν_{ur}	φ (°)	ψ (°)	R_f
80	18.2	48 000	48 000	144 000	0.450	0.2	38	8	0.9

increase in mean effective stress on the pile with L/D = 3 is broadly the same as that of the pile with L/D = 5. This is likely a result that the applied vertical loading, $0.2V_u$ is proportional to the ultimate capacity of each pile.

Similar to the evaluation of the influence of applied vertical loading on the soil resistance (eq. 2), the effect of vertical loading on the mean effective stress can be quantified using the following equation:

$$\zeta = \frac{\sigma_{m,V} - \sigma_{m,0}}{\sigma_{m,0}} \quad (3)$$

where ζ is defined as the improvement in mean effective stress due to the application of vertical loading, $\sigma_{m,0}$ is the mean effective stress under zero vertical loading, and $\sigma_{m,V}$ is the mean effective stress when the applied vertical load is a non-zero value.

Figures 18*a* and 18*b* present plots of the improvement in mean effective stress under the influence of vertical loading along the pile embedded length for piles with L/D = 5 and L/D = 3 respectively. Data clearly show that the increase of vertical load increases the mean effective stress at all soil depths along both piles.

4.3. Change in mean effective stress under vertical loading at a lateral displacement 0.1*D*

At an imposed lateral displacement of 0.1*D* and under the action of vertical loading ($0.2V_u$), the change in mean effective stress measured near the pile in the *XZ*-plane is shown in Fig. 19 for piles with L/D of 5 and 3. The change in mean effective stress is once again obtained by subtracting the mean effective stress profile corresponding to the initial unloaded condition (no *V*) from that corresponding to the applied vertical load of $0.2V_u$. It should be noted that the loads are applied similar to the load application sequence described in the experimental investigation, namely that vertical loading is applied prior to imposing a lateral displacement. It can be observed that at the imposed lateral displacement (0.1*D*) the mean effective stress level increases substantially in the region surrounding each pile once the vertical loading is applied, which helps to explain the increased pile capacity observed under the action of vertical loading in the experimental investigation (Fig. 8).

Fig. 17. Change in mean effective stress in the *XZ*-plane by applying a vertical load of $0.2V_u$: (*a*) L/D = 5 and (*b*) L/D = 3. [Colour online.]

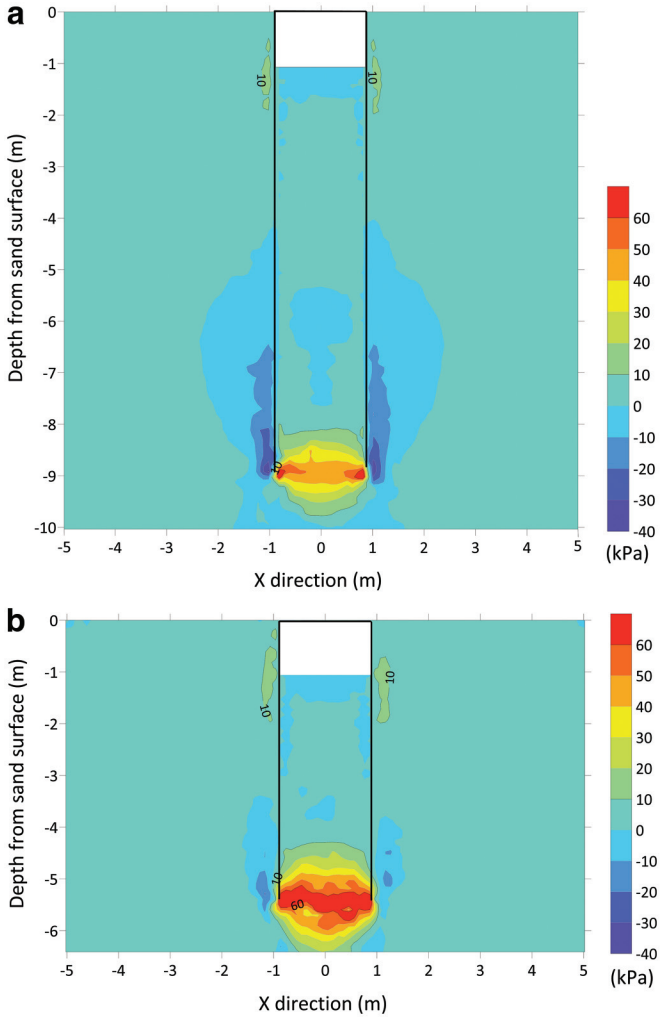

Fig. 18. Improvement in mean effective stress under applied vertical loads along depth of piles: (*a*) $L/D = 5$ and (*b*) $L/D = 3$. [Colour online.]

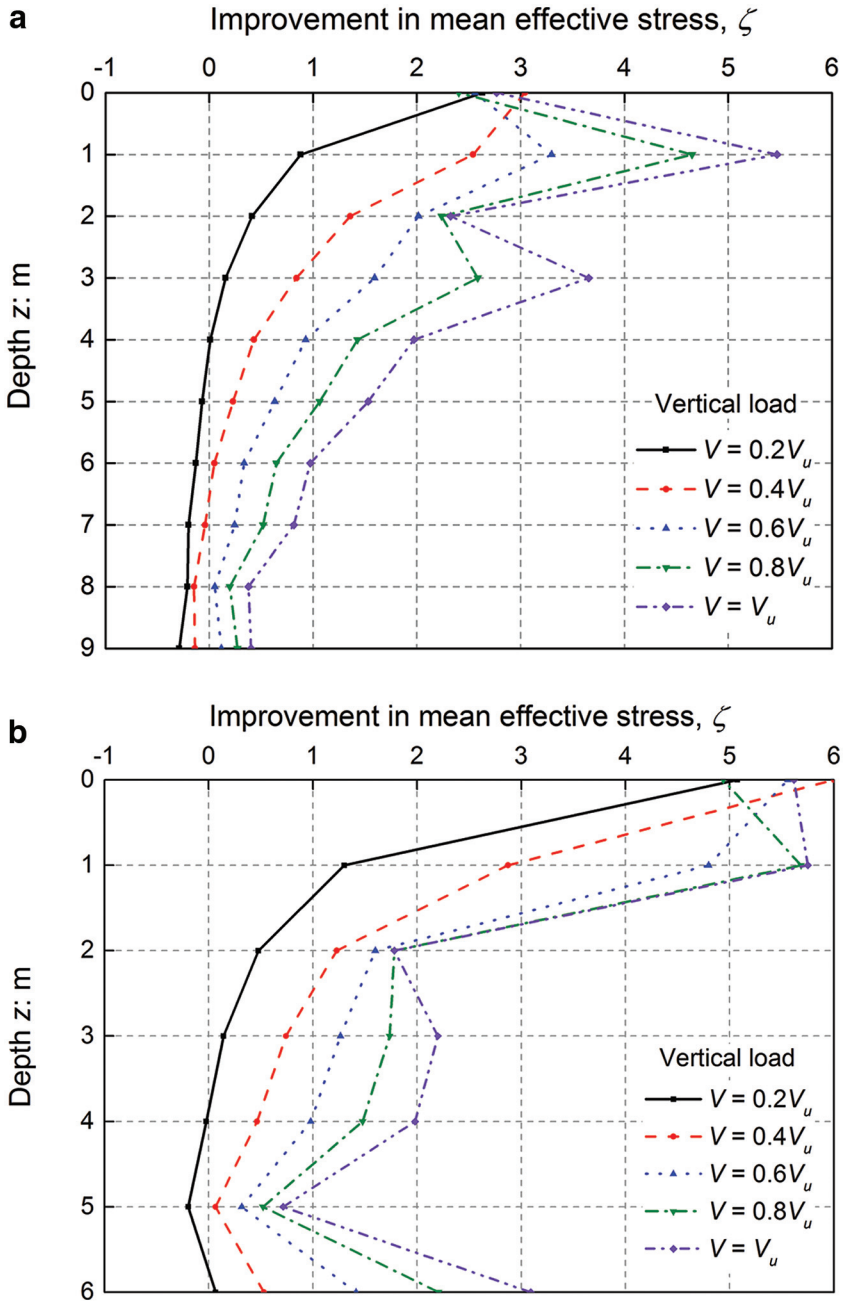

The same information as shown in Fig. 19 for the pile elevations is also shown in plan view in the supplementary files (see Fig. S2),[1] corresponding to a depth of 1.5*D* (2.7 m) in the ground. Figure S2*a*[1] shows the data for the pile with $L/D = 5$, and Fig. S2*b*[1] shows that for the pile with $L/D = 3$. The mean effective stress generated around both piles increases significantly due to the application of vertical loading.

The numerical simulations serve the purpose of qualitatively explaining the mechanism underlying the observed behaviour in the experimental tests conducted in this paper, namely that the increased mean effective stress caused by the application of vertical loading increases the lateral capacity of the piles under subsequent applied lateral loading. The numerical analyses are not intended to explicitly model the conditions in the tests conducted, but to be representative of typical conditions.

5. Conclusions

In this study, an investigation into the influence of vertical loading on the lateral response features of monopiles is conducted using physical (centrifuge) modelling. A series of vertical, lateral and combined load tests were performed on piles installed at 1g and 100g (in-flight) in dry dense sand ($D_r = 80\%$). Numerical simulations were performed to obtain a qualitative understanding of the underlying mechanism on how vertical loading affects pile lateral behaviour. Two different L/D ratios were considered to investigate the effect of pile slenderness. The conclusions drawn from this study can be summarized as follows:

1. The application of vertical loading is beneficial to the lateral load capacity and stiffness of piles with L/D in the range 3–5.

Fig. 19. Change in mean effective stress in the *XZ*-plane at lateral displacement 0.1*D* by applying a vertical load of $0.2V_u$: (*a*) $L/D = 5$ and (*b*) $L/D = 3$. [Colour online.]

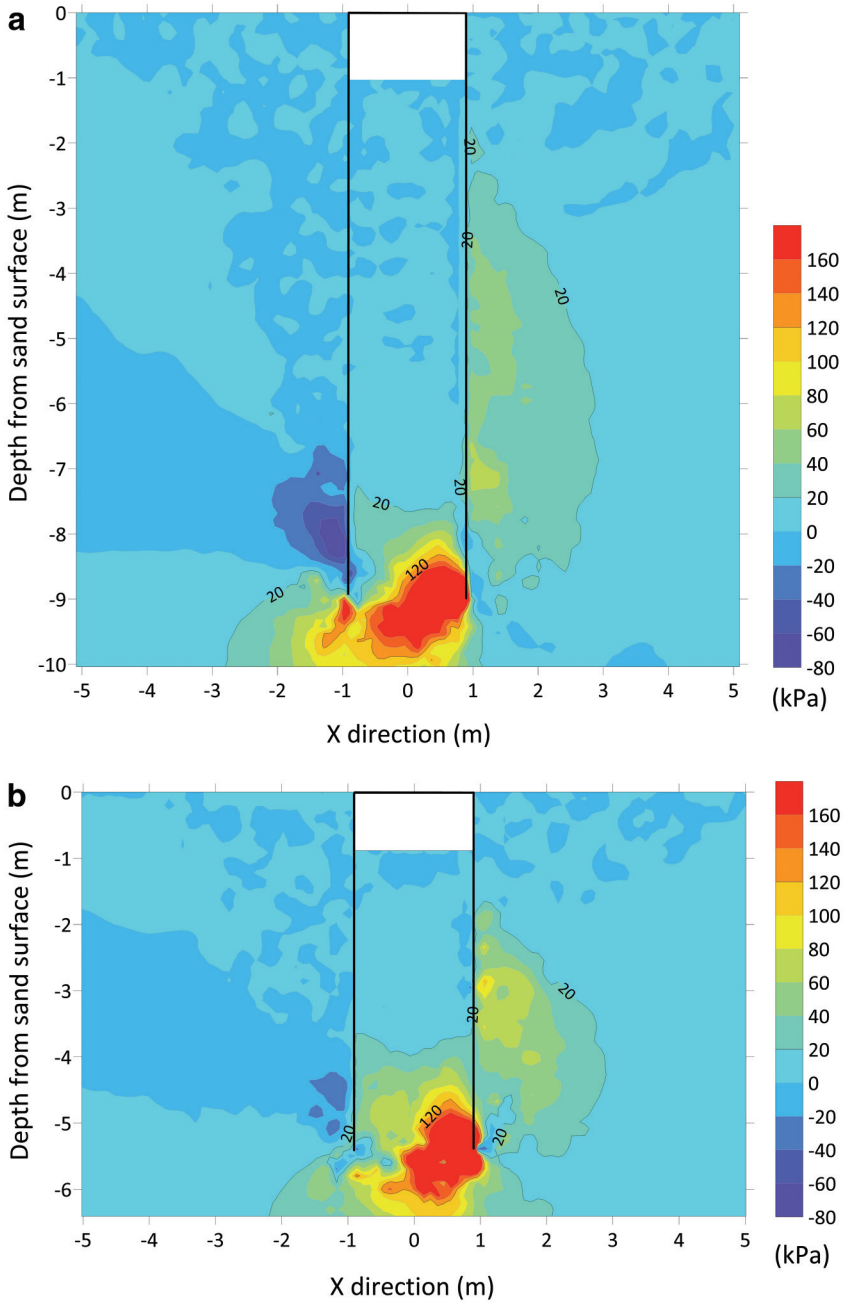

2. For piles with an L/D ratio of 5, the beneficial effect of vertical loading increases as the ratio of V/V_u increases.
3. For piles with $L/D = 3$ the lateral capacity increases initially as the vertical load increases. The normalized pile lateral capacity reaches a peak value when the vertical load is between $0.4V_u$ and $0.5V_u$. For higher vertical loads the beneficial effect of vertical loading reduces.
4. Notwithstanding this the net benefit to the lateral capacity on piles with $L/D = 3$ is higher than for a pile with $L/D = 5$ when the ratio V/V_u is below 0.8.
5. For a pile with $L/D = 5$, the normalised lateral soil resistance p/D measured at a normalised lateral displacement of $0.01D$ increases approximately linearly as V/V_u increases.
6. The data show that the method of pile installation has a clear influence on the stiffness and lateral bearing resistance of the piles tested in this study. Installing the piles in-flight leads to a higher retention of lateral effective stress and denser surrounding sand, which manifest as a larger initial stiffness and higher lateral resistance at corresponding displacements than for piles pre-installed at 1g.

The test results suggest that the influence of vertical loading on the pile lateral capacity is dependent on the pile L/D ratio. A comparison of the experimental p–y curves reveals that application of vertical loading increases both the stiffness of the p–y curves and the soil resistance. An analysis of the influence of pile installation method on resulting p–y curves was not possible as the instrumented pile could not be installed in-flight due to the potential to damage the instrumentation. The mechanism underlying the observed behaviour is investigated by developing

numerical models of both piles (L/D = 5 and 3) using PLAXIS. It is demonstrated that under the action of applying vertical loads, the change in mean effective stress level in the vicinity surrounding each pile is likely responsible for the increased stiffness observed in the experimental tests. Future work will focus on quantifying the benefits obtained under combined loading conditions in a design framework.

Acknowledgements

This work is funded by the Section of Geo-Engineering, Delft University of Technology. The first author received support from the China Scholarship Council (CSC).

References

Achmus, M. 2010. Design of axially and laterally loaded piles for the support of offshore wind energy converters. *In* Proceedings of the Indian Geotechnical Conference GEOtrendz-2010, Mumbai, India. pp. 92–102.

Allersma, H. 1994. The University of Delft geotechnical centrifuge. Centrifuge, **94**: 47–52.

API. 2011. API 2GEO (2011) Geotechnical and foundation design considerations. American Petroleum Institute, Washington, D.C., USA.

Bransby, M., and Randolph, M. 1998. The effect of skirted foundation shape on response to combined V-MH loadings. *In* Proceedings of the Eighth International Offshore and Polar Engineering Conference. International Society of Offshore and Polar Engineers.

Brinkgreve, R., Engin, E., and Engin, H. 2010. Validation of empirical formulas to derive model parameters for sands. *In* Numerical methods in geotechnical engineering. pp. 137–142.

Brinkgreve, R., Kumarswamy, S., and Swolfs, W. 2015. Plaxis 3D anniversary edition manual. Plaxis BV, Delft, the Netherlands.

Butterfield, R., and Gottardi, G. 1994. A complete three-dimensional failure envelope for shallow footings on sand. Géotechnique, **44**(1): 181–184. doi:10.1680/geot.1994.44.1.181.

Byrne, B.W., Burd, H.J., Zdravković, L., McAdam, R.A., Taborda, D.M., Houlsby, G.T., et al. 2019. PISA: new design methods for offshore wind turbine monopiles. Revue Française de Géotechnique, **158**: 3. doi:10.1051/geotech/2019009.

Choo, Y.W., and Kim, D. 2016. Experimental development of the *p-y* relationship for large-diameter offshore monopiles in sands: centrifuge tests. Journal of Geotechnical and Geoenvironmental Engineering, **142**(1): 04015058. doi:10.1061/(ASCE)GT.1943-5606.0001373.

Chortis, G., Askarinejad, A., Prendergast, L., Li, Q., and Gavin, K. 2020. Influence of scour depth and type on *p-y* curves for monopiles in sand under monotonic lateral loading in a geotechnical centrifuge. Ocean Engineering, **197**: 106838. doi:10.1016/j.oceaneng.2019.106838.

De Jager, R.R., Maghsoudloo, A., Askarinejad, A., and Molenkamp, F. 2017. Preliminary results of instrumented laboratory flow slides. *In* Proceedings of the 1st International Conference on the Material Point Method. Elsevier Ltd., Delft, the Netherlands.

De Nicola, A. 1996. The performance of pipe piles in sand. Doctoral dissertation, University of Western Australia, Perth, Australia.

De Nicola, A., and Randolph, M.F. 1997. The plugging behaviour of driven and jacked piles in sand. Géotechnique, **47**(4): 841–856. doi:10.1680/geot.1997.47.4.841.

Doherty, P., and Gavin, K. 2012. Laterally loaded monopile design for offshore wind farms. Proceedings of the Institution of Civil Engineers – Energy, **165**(1): 7–17. doi:10.1680/ener.11.00003.

Dyson, G.J., and Randolph, M.F. 2001. Monotonic lateral loading of piles in calcareous sand. Journal of Geotechnical and Geoenvironmental Engineering, **127**(4): 346–352. doi:10.1061/(ASCE)1090-0241(2001)127:4(346).

Fan, S., Bienen, B., and Randolph, M.F. 2021. Centrifuge study on effect of installation method on lateral response of monopiles in sand. International Journal of Physical Modelling in Geotechnics, **21**: 40–52. doi:10.1680/jphmg.19.00013.

Garnier, J., Gaudin, C., Springman, S.M., Culligan, P., Goodings, D., Konig, D., et al. 2007. Catalogue of scaling laws and similitude questions in geotechnical centrifuge modelling. International Journal of Physical Modelling in Geotechnics, **7**(3): 1–23. doi:10.1680/ijpmg.2007.070301.

HT Sensor Technology Co., Ltd. 2021. HTC-SENSOR TAL220. Available from http://www.htc-sensor.com/products/162.html.

ISO. 2016. ISO 19901-4. Petroleum and natural gas industries - Specific requirements for offshore structures - Part 4: Geotechnical and foundation design considerations. Available from https://www.iso.org/standard/61144.html.

Jain, N., Ranjan, G., and Ramasamy, G. 1987. Effect of vertical load on flexural behaviour of piles. Geotechnical Engineering, **18**(2): 185–204.

Karasev, O., Talanov, G., and Benda, S. 1977. Investigation of the work of single situ-cast piles under different load combinations. Soil Mechanics and Foundation Engineering, **14**(3): 173–177. doi:10.1007/BF02092686.

Karthigeyan, S., Ramakrishna, V., and Rajagopal, K. 2007. Numerical investigation of the effect of vertical load on the lateral response of piles. Journal of Geotechnical and Geoenvironmental Engineering, **133**(5): 512–521. doi:10.1061/(ASCE)1090-0241(2007)133:5(512).

Klinkvort, R., and Hededal, O. 2010. Centrifuge modelling of offshore monopile foundation. *In* Frontiers in offshore Geotechnics II: Proceedings of the 2nd International Symposium Frontiers in Offshore Geotechnics (ISFOG2010). *Edited by* S.M. Gourvenec and D. White. Taylor and Francis, London, U.K. pp. 581–586.

Lee, J. 2008. Experimental investigation of the load response of model piles in sand. Ph.D. thesis, Purdue University.

Li, Q., Prendergast, L., Askarinejad, A., and Gavin, K. 2018. Effect of scour on the behavior of a combined loaded monopile in sand. *In* Proceedings of the 9th European Conference on Numerical Methods in Geotechnical Engineering, Porto, Portugal.

Li, Q., Askarinejad, A., and Gavin, K. 2020*a*. Lateral response of rigid monopiles subjected to cyclic loading: centrifuge modelling. Proceedings of the Institution of Civil Engineers - Geotechnical Engineering. [Published online ahead of print 16 December 2020.] doi:10.1680/jgeen.20.00088.

Li, Q., Prendergast, L., Askarinejad, A., and Gavin, K. 2020*b*. Influence of vertical loading on behavior of laterally-loaded foundation piles: a review. Journal of Marine Science and Engineering, **8**(12): 1029. doi:10.3390/jmse8121029.

Li, Q., Prendergast, L., Askarinejad, A., Chortis, G., and Gavin, K. 2020*c*. Centrifuge modeling of the impact of local and global scour erosion on the monotonic lateral response of a monopile in sand. Geotechnical Testing Journal, **43**: 1084–1100. doi:10.1520/GTJ20180322.

Li, Q., Askarinejad, A., and Gavin, K. 2021. The impact of scour on the lateral resistance of wind turbine monopiles: an experimental study. Canadian Geotechnical Journal, **58**(11): 1770–1782. doi:10.1139/cgj-2020-0219.

Lu, W., and Zhang, G. 2018. Influence mechanism of vertical-horizontal combined loads on the response of a single pile in sand. Soils and Foundations, **58**(5): 1228–1239. doi:10.1016/j.sandf.2018.07.002.

Maghsoudloo, A., Askarinejad, A., De Jager, R., Molenkamp, F., and Hicks, M. 2018. Experimental investigation of pore pressure and acceleration development in static liquefaction induced failures in submerged slopes. *In* Physical modelling in geotechnics. Vol. 2. CRC Press.

McAdam, R.A., Byrne, B.W., Houlsby, G.T., Beuckelaers, W.J., Burd, H.J., Gavin, K.G., et al. 2019. Monotonic laterally loaded pile testing in a dense marine sand at Dunkirk. Géotechnique, **70**: 986–998. doi:10.1680/jgeot.18.PISA.004.

Mu, L., Kang, X., Feng, K., Huang, M., and Cao, J. 2018. Influence of vertical loads on lateral behaviour of monopiles in sand. European Journal of Environmental and Civil Engineering, **22**(sup1): s286–s301. doi:10.1080/19648189.2017.1359112.

Murphy, G., Igoe, D., Doherty, P., and Gavin, K. 2018. 3D FEM Approach for Laterally Loaded Monopile Design. Computers and Geotechnics, **100**: 76–83. doi:10.1016/j.compgeo.2018.03.013.

Nova, R., and Montrasio, L. 1991. Settlements of shallow foundations on sand. Géotechnique, **41**(2): 243–256. doi:10.1680/geot.1991.41.2.243.

Nunez, I., Hoadley, P., Randolph, M., and Hulett, J. 1988. Driving and tension loading of piles in sand on a centrifuge. Centrifuge, **88**: 353–362.

Prakasha, K., Joer, H., and Randolph, M. 2005. Establishing a model testing capability for deep water foundation systems. *In* Proceedings of the 15th International Offshore and Polar Engineering Conference and Exhibition, Seoul, Korea. pp. 309–315.

Qi, W., Gao, F., Randolph, M., and Lehane, B. 2016. Scour effects on p-y curves for shallowly embedded piles in sand. Géotechnique, **66**(8): 648–660. doi:10.1680/jgeot.15.P.157.

SIMBATOUCH SBT620. 2021. Available from https://www.china.cn/chengzhongchuanganqi/4378290334.html.

WindEurope. 2018. Offshore wind in Europe: Key trends and statistics 2017.

Xue, J., Gavin, K., Murphy, G., Doherty, P., and Igoe, D. 2016. Optimization technique to determine the *p-y* curves of laterally loaded stiff piles in dense sand. Geotechnical Testing Journal, **39**(5): 842–854. doi:10.1520/GTJ20140257.

Yang, K., and Liang, R. 2006. Methods for deriving *p-y* curves from instrumented lateral load tests. Geotechnical Testing Journal, **30**(1): 31–38. doi:10.1520/GTJ100317.

Zhang, W., and Askarinejad, A. 2019*a*. Behaviour of buried pipes in unstable sandy slopes. Landslides, **16**(2): 283–293. doi:10.1007/s10346-018-1066-1.

Zhang, W., and Askarinejad, A. 2019*b*. Centrifuge modelling of submarine landslides due to static liquefaction. Landslides, **16**(10): 1921–1938. doi:10.1007/s10346-019-01200-z.

List of symbols

C_C	curvature coefficient of sand
C_U	uniformity coefficient of sand
D	pile outer diameter
D_{50}	average grain size of sand
D_r	relative density of sand
E	Young's modulus
E_{50}^{ref}	secant stiffness for CD triaxial test
E_{oed}^{ref}	tangent oedometer stiffness
E_{ur}^{ref}	unloading reloading stiffness
e	load eccentricity
e_{max}	maximum void ratio of sand

e_{min} minimum void ratio of sand
Gs specific gravity of sand
g gravitational acceleration rate
H lateral load
H_u pile lateral capacity
$H_{u,0}$ pile lateral capacity under zero vertical loading
$H_{u,V}$ pile lateral capacity when the applied vertical load is a nonzero value
I moment of inertia
k stiffness
k_{ini} initial stiffness
L pile embedded length
L_T total length of model monopile
M bending moment
m power of stress-level dependency of stiffness
P1 pile No. 1
P2 pile No. 2
P3 pile No. 3
p lateral soil resistance
p_0 lateral soil resistance under zero vertical loading
p_V lateral soil resistance when the applied vertical load is a nonzero value
R_0 distance from pile pivot point to pile toe
R_f failure ratio
R_{inter} relative strength of the interface to soil
s penetration depth
t pile wall thickness
V vertical load
V_u pile vertical capacity
V_{u_pre} pile vertical capacity on pre-installed pile
y lateral displacement
z depth in the soil from mudline
α pile rotation angle
γ unit weight of sand
γ' effective unit weight of sand
ϑ normalized pile lateral capacity
ν Poisson's ratio
ν_{ur} Poisson's ratio for unloading–reloading
$\sigma_{m,0}$ mean effective stress under zero vertical loading
$\sigma_{m,V}$ mean effective stress when the applied vertical load is a nonzero value
ζ improvement in mean effective stress
φ friction angle of sand in numerical simulation
φ_{cr} critical friction angle of sand in physical modelling
χ improvement in soil resistance
ψ angle of dilation